Accelerated Kinetics Revealing Metastable Pathways of Magnesiation-Induced Transformations in MnO_2 Polymorphs

Takuya Hatakeyama,* Hongyi Li, Norihiko L. Okamoto, Kohei Shimokawa, Tomoya Kawaguchi, Hiroshi Tanimura, Susumu Imashuku, Maximilian Fichtner, and Tetsu Ichitsubo*

ABSTRACT: The intrinsic potential of manganese dioxides, considered high capacity cathodes of rechargeable magnesium batteries, was clearly exposed under conditions where the Mg migration kinetics are sufficiently enhanced. It has been reported to date that magnesium insertion into MnO_2 is substantially confined to the surfaces of MnO_2 particles due to its sluggish kinetics at room temperature, which leads to local overmagnesiation conditions causing conversion reactions etc. To unveil its ergodic or metastable phase transformation pathways of MnO_2 polymorphs (α, β, γ, δ, and λ) during magnesiation, this study employed intermediate temperature electrochemical experiments (at 150 °C) using heat tolerant ionic liquid electrolytes. Regardless of its original polymorphic structure, each MnO_2 polymorph was found to transform into a Mg including spinel and then to a rocksalt like phase by magnesiation. Given this tendency of transformation, the defect spinel λ MnO_2 phase possessing the coherent framework of spinel/rocksalt structures is expected to follow a topotactic transformation pathway, but thermally unstable λ MnO_2 underwent spontaneous reduction into Mn_3O_4 before magnesiation in an electrolyte. Instead, α MnO_2 was found to be robust enough among MnO_2 polymorphs to exhibit reversible magnesium intercalation at 150 °C under limiting capacity conditions. This result highlights that reversible magnesium intercalation in oxide cathodes is feasible for structures that are kinetically resistant to irreversible transformation pathways to spinel and rocksalt structures.

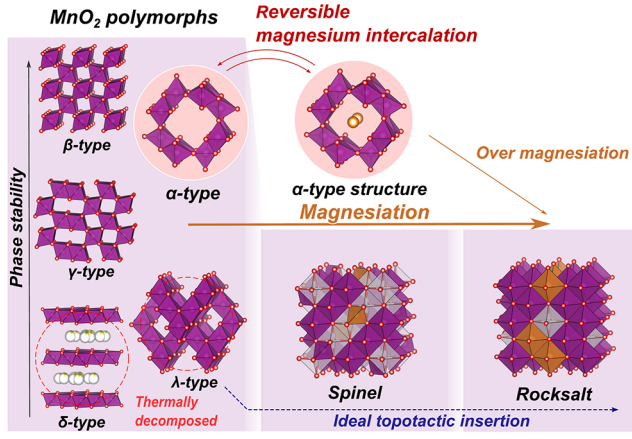

1. INTRODUCTION

Rechargeable magnesium batteries (RMBs) that employ magnesium metal anodes are potential alternatives to currently available Li based batteries.[1−3] The major advantages of Mg metal are its natural abundance in the earth's crust compared to Li, the high volumetric capacity, and the dendrite free deposition upon charging.[4] Therefore, constructing RMBs can potentially save material costs compared to Li ion batteries (LIBs) and offer a long term option for battery technology in general. The Mg metal anode yields an ideal capacity (volumetric, 3833 mAh/cm^3; gravimetric, 2205 mAh/g) much higher than that of graphite (746 mAh/cm^3, 370 mAh/g) and comparable to that of Li metal (2062 mAh/cm^3, 3860 mAh/g). Moreover, magnesium tends to be plated rather smoothy during its electrodeposition,[4] thereby ensuring safe operation in contrast to Li metal that easily forms dendrites.

Development of RMBs has, however, been impeded by a lack of promising cathode materials. Our group substantiated that spinel type oxides such as MgX_2O_4 (X = Co, Mn, etc.) can accommodate sufficient Mg ions via spinel to rocksalt transition, in which rocksalt type $Mg_2X_2O_4$ is formed through electrochemical magnesiation at elevated temperatures.[5] Since spinel and rocksalt structures can coherently share a common anion sublattice (assigned by 32e sites of space group #227), Mg intercalation/deintercalation reversibly proceeds through semicoherent phase transformation between spinel and rocksalt phases. In this mechanism, Mg ions inserted into 16c vacant sites of a spinel structure "push out" Mg ions located at 8a tetrahedral sites to 16c octahedral sites, and a rocksalt phase is eventually formed by disordering of Mg and X (X = Co, Mn, etc.) located at octahedral sites (16c and 16d, respectively). Although the phase transformation between spinel and rocksalt makes Mg insertion obviously appreciable, this somewhat complicated process impedes capacity retention. To overcome this problem, we recently proposed defect spinel

type $ZnMnO_3$ as a new cathode material for RMBs that can enable prolonged capacity retention.[6] Because $ZnMnO_3$ originally includes cation defects at 16d sites, Mg insertion into $ZnMnO_3$ does not any longer require the push out process that would hinder reverting. Since $ZnMnO_3$ can be regarded as a mixture of ZnO and MnO_2, the structure stability of magnesiated MnO_2 deserves to be investigated for further progress of the RMB cathode materials.

The advantages of MnO_2 cathodes are (1) a high voltage derived from the valence change of $Mn^{4+/3+}$, (2) a large gravimetric capacity of 616 mAh/g using also a $Mn^{3+/2+}$ redox reaction (based on the mass of MnO_2), and (3) a wide choice from various polymorphic crystal structures. As is well known, MnO_2 has various polymorphs, so that it offers a wide choice of crystal structures such as α (hollandite, space group: $I4/m$), β (pyrolusite, $P4_2/mnm$), R (ramsdellite, $Pnma$), γ (mixture of β and R), δ (birnessite, $C2/m$), and λ (spinel, $Fd3m$). As to the Li intercalation into MnO_2 polymorphs, Thackeray deeply investigated, considered, and summarized their lithiation behaviors in a review paper.[7] The feasibility of the $Mn^{4+/3+}$ redox reaction has been proven with electrochemical insertion of two Li's into spinel λ Mn_2O_4 to form spinel $LiMn_2O_4$ (4.2−3.5 V vs Li^+/Li) and subsequently spinel $Li_2Mn_2O_4$ (2.8 V vs Li^+/Li).[8,9] Additionally, further electrochemical lithiation of spinel (λ) $Li_2Mn_2O_4$ allows the $Mn^{3+/2+}$ redox reaction to form layered $Li_4Mn_2O_4$ (around 1.2 V vs Li^+/Li).[7]

The feasibility of magnesiation in MnO_2 polymorphs has been examined by many researchers. Among the different polymorphs, especially λ type (spinel type) MnO_2 has been intensively investigated with respect to the ability of Mg intercalation[10−16] due to its structural similarity to $LiMn_2O_4$. In our previous studies,[17] Mg intercalation in tetragonal spinel $MgMn_2O_4$ was demonstrated in ionic liquid heated up to 150 °C. The demagnesiation process of spinel $MgMn_2O_4$ proceeds through a two phase reaction between tetragonal spinel $MgMn_2O_4$ and cubic spinel $Mg_{1-x}Mn_2O_4$, involving the redox of $Mn^{4+/3+}$. Additionally, Mg insertion into tetragonal spinel $MgMn_2O_4$ allows the redox of $Mn^{3+/2+}$ accompanied by coherent phase transformation into rocksalt $Mg_{1+x}Mn_2O_4$.[5] Since birnessite type δ MnO_2 is stabilized by structural water in the interlayers, the electrochemical Mg intercalation in δ MnO_2 has been reported mainly for aqueous electrolytes. δ MnO_2 provides a magnesiation capacity of around 150 mAh/g through reversible layered to spinel phase transformation.[18−21] α MnO_2 shows high capacity around 280 mAh/g on the initial discharge even at room temperature in Mg containing electrolytes,[22,23] although this high capacity of α MnO_2 has been attributed to an irreversible conversion reaction rather than intercalation.[24−26] Thus, the rapid capacity fade of MnO_2 cathodes is considered to be caused by irreversible phase transformation especially when cycled in nonaqueous electrolytes.

Also from the thermodynamic aspects, given the stable compounds of the Mg−Mn−O system, possible products are expected to be rocksalt MgO + bixbyite Mn_2O_3, rocksalt MgO + spinel Mn_3O_4, rocksalt MgO + rocksalt MnO, spinel $MgMn_2O_4$, and rocksalt $MgMnO_2$. In fact, a computational study by Ling et al.[26] suggested the instability of Mg inserted (magnesiated) α MnO_2 against possible conversion products over a wide Mg concentration range. Similarly, calculation data provided by Kitchaev et al.[27] can be interpreted as the instability of magnesiated polymorph MnO_2 against spinel $MgMn_2O_4$ and rocksalt MgO + MnO. Using DFT calculation, Canepa et al. also indicated that oxide intercalation hosts tend to prefer a conversion reaction rather than an intercalation reaction due to the large formation energy of MgO.[28]

Despite these attempts to explain the instability of magnesiated MnO_2 structures, the experimental observations related to the decomposition product of magnesiated MnO_2 are limited to only a few examples. Pioneering work by Arthur et al.[25] using transmission electron microscopy demonstrated that Mg insertion into α MnO_2 results in the formation of an amorphous (Mg, Mn)O layer on the surface of α MnO_2 particles. This result basically suggests that α MnO_2 (including the other polymorphs of MnO_2) would be unable to incorporate Mg via intercalation reaction. However, when considering the high activation energy of magnesium insertion, accelerated kinetics are expected to change the reaction pathways not only of α MnO_2 but also of the other MnO_2 polymorphs. From this standpoint, magnesiation induced transformation behaviors of MnO_2 polymorphs are still unclear due to insufficient kinetics. This study aims to expose *ergodic* pathways (which means that a system has a capability of sampling the possible states to seek an equilibrium or metastable states in a kinetically enhanced condition) of magnesiation induced phase transformations of MnO_2 polymorphs experimentally and to discuss the experimental transformation behaviors by comparing the thermodynamic viewpoint predicted from the ab initio calculations.

2. RESULTS

2.1. Fabrication and Sample Characterization of Pristine MnO_2 Polymorphs. To experimentally investigate phase change behavior of magnesiated MnO_2 polymorphs, we prepared α , β , γ , δ , and λ MnO_2. Here, we substituted the γ phase (mixture of 2 × 2 and 1 × 1 domains) for the R phase (2 × 2 structure) because a pure R phase without a 1 × 1 domain is difficult to obtain from laboratory synthesis. α , β , and γ MnO_2 were synthesized through the hydrothermal method; λ MnO_2 was produced from spinel $LiMn_2O_4$ through chemical extraction of Li using HCl solution, and δ MnO_2 was prepared from $KMnO_4$ by thermal decomposition and washing with distilled water. Although the host structures of λ MnO_2 and δ MnO_2 were not completely emptied, compositional analysis (based on inductivity coupled plasma, ICP, optical emission spectrometry) confirmed that Li and K content in the bulk composition were reduced by the solution treatment up to λ $Li_{0.1}MnO_2$ and δ $K_{0.3}MnO_2$, respectively.

X ray diffraction patterns of prepared MnO_2 polymorphs (Figure 1) generally agree well with the respective reference patterns. γ MnO_2 is known to consist of the R MnO_2 (2 × 1) structure, including microdomains of β MnO_2 (1 × 1) units.[29] The difference between experimental diffraction pattern of γ MnO_2 and the calculated diffraction pattern of R MnO_2 can be attributed to the presence of β MnO_2 (1 × 1) microdomains. An XRD simulation that takes microdomains into account (Figure S1) indicated that the prepared γ MnO_2 comprised approximately 80 vol % of the ramsdellite (R) domains separated by 20 vol % of pyrolusite (β) domains. Furthermore, the oxidation of manganese in λ (Li)MnO_2 was suggested by the initial electrode potential (see Figure 2a later) to be higher than that of $LiMn_2O_4$ (ca. 3.0 V vs Li) and also the shrinkage of the lattice constant (the pristine $LiMn_2O_4$ shows a = 8.24 Å, whereas the Li extracted λ Mn_2O_4 immersed in an HCl solution has a smaller one, a = 8.05 Å). These properties of

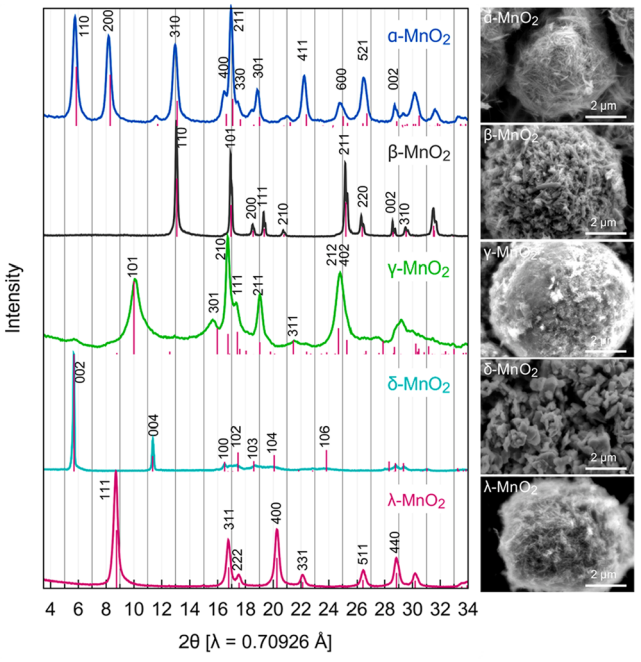

Figure 1. XRD and SEM images of various kinds of MnO_2 polymorphs prepared in this work. Red bars show reference diffraction patterns of α MnO_2 (ICSD 20227), β MnO_2 (ICSD 393), R MnO_2 (ICSD 171866), λ MnO_2 (ICSD 193445), and δ MnO_2 (ICSD 55411). Diffraction peaks of α, β, γ, δ, and λ type structures are indexed based on space group symmetry $I4/m$, $P4_2/mnm$, $Pnma$, $P6_3/mmc$, and $Fd3m$, respectively.

the Li extracted Mn_2O_4 are in very good agreement with the previous results.[30]

2.2. Accelerated Electrochemical Mg Insertion into Various MnO_2 Polymorphs at 150 °C and Their Transformation Behaviors. Electrochemical properties of MnO_2 polymorphs were examined by cyclic voltammetry measurements (Figure S2) and galvanostatic discharge (Figure 2). The experiments were conducted with a three electrode beaker cell heated up to 150 °C to enhance Mg insertion kinetics that are usually sluggish at room temperature. We employed an ionic liquid electrolyte $Mg(TFSA)_2$/CsTFSA (molar ratio Mg/Cs = 1/9) that exhibits low volatility even at 150 °C. Note here that the electrode potential was measured against a Li metal electrode separated from a Mg electrolyte; this setup has already been examined in our previous works. The redox potential of Mg^{2+}/Mg was determined to be about 0.5 V versus Li^+/Li in the Mg−Cs ionic liquid electrolyte.[5,6,31] The Li reference was used to overcome the problem of the passivation of the Mg metal electrode with the TFSA anion so that accurate redox potentials cannot be measured by using a conventional Mg ribbon reference. In a very condensed Mg electrolyte like this ionic liquid, the Li contamination from the reference electrode can be neglected in most cases.

Phase transformation behavior of magnesiated MnO_2 polymorphs was investigated using XRD measurement after electrochemical magnesiation at 150 °C. As shown in Figure 2a, MnO_2 electrodes were galvanostatically discharged up to 2.0 V vs Li^+/Li (about 1.5 V vs Mg^{2+}/Mg) after a preliminary charge to remove residual ions within MnO_2 structures. Figure 2b−f show the XRD profiles for each discharge amount and corresponding structures. As seen in Table 1, an increase in the Mg concentration after discharge was confirmed by ICP analysis. Even though the ionic liquid electrolyte contains more Cs^+ ions (Mg/Cs = 1:9), the Cs concentration in the discharged MnO_2 electrode is negligible compared to the Mg concentration. The CV profile (Figure S3) in CsTFSA electrolyte not containing $Mg(TFSA)_2$ also suggests that a reaction involving Cs is not dominant in the case of $Mg(TFSA)_2$/CsTFSA electrolyte. We tried to employ a $Mg(TFSA)_2$/PP13TFSA electrolyte for magnesiation (see Table S1 and Figure S4); however, the Mg content of the MnO_2 electrode after discharge was much smaller than what was expected based on discharge capacity. This is presumably due to side reactions such as electrolyte decomposition and proton insertion in the PP13 based electrolyte. We therefore chose the $Mg(TFSA)_2$/CsTFSA electrolyte that reasonably allows magnesiation.

2.2.1. α-MnO_2. As shown in Figure 2a, α MnO_2 shows a discharge capacity of 280 mAh/g (~0.45 Mg per MnO_2). In the present experiments on α MnO_2, Li contamination can be thoroughly neglected since Li could not be detected in the ICP analysis as seen in Table 1. The XRD patterns in Figure 2b indicate that a high degree of magnesiation up to 280 mAh/g induces transformation of α MnO_2 ($I4/m$) into a "rocksalt like" single phase even far below the rocksalt composition. This intriguing behavior is observed also in γ MnO_2 and is discussed in a later section.

Before the transformation to the rocksalt like phase occurs, the XRD peaks of the magnesiated α MnO_2 shift to lower angles compared to pristine α MnO_2. The most important characteristic feature in the XRD profile change is a decrease in the intensities of 110 and 200 diffraction peaks relative to that of the 130 diffraction peak. Figure 3a shows the Rietveld analysis for the pristine α MnO_2 and the intensity simulation profiles for various Mg sites using the Debye−Waller parameter obtained by the fitting process for the pristine sample (see Table S2). The above experimental trend can be interpreted by assuming that the inserted Mg ions are located at or around the center position of the 2 × 2 tunnel of α MnO_2 (2a, 2b, or 8h in $I4/m$) as demonstrated in Figure 3b and Figure S7. Thus, it is indicated that α MnO_2 topotactically accommodates Mg up to 220 mAh/g (~0.36 Mg per MnO_2) via solid solution mechanism.

2.2.2. β-MnO_2. After being soaked for 44 h in the electrolyte, as is seen in Figure 2c, a small new diffraction peak around 12.0° appeared; it could not be identified due to lack of other distinct peaks. Nevertheless, this phase is surely robust even at 150 °C.

Since β MnO_2 is the most dense and is well known as the most stable phase among the polymorphs, it is expected that Mg insertion may not be possible. However, β MnO_2 shows a fairly large capacity of 170 mAh/g (~0.28Mg per MnO_2) at 150 °C (Figure 2a). The X ray diffraction measurement upon magnesiation also indicates the appearance of a secondary phase coexisting with pristine β MnO_2. Here, it should be noted that we also have to take account of Li insertion. As shown in Table 1, about 19% of the capacity is contributed by the Li insertion, while most of the carrier ions could be regarded as Mg ions. As far as we know, it is the first report on Mg insertion into (or reaction with) β MnO_2. There are two possible reasons why Mg insertion can be attained in this experiment: (i) facilitated kinetics of Mg insertion at elevated temperature (150 °C) and (ii) the concerted interaction with monovalent mobile Li ions and divalent sluggish Mg ions,

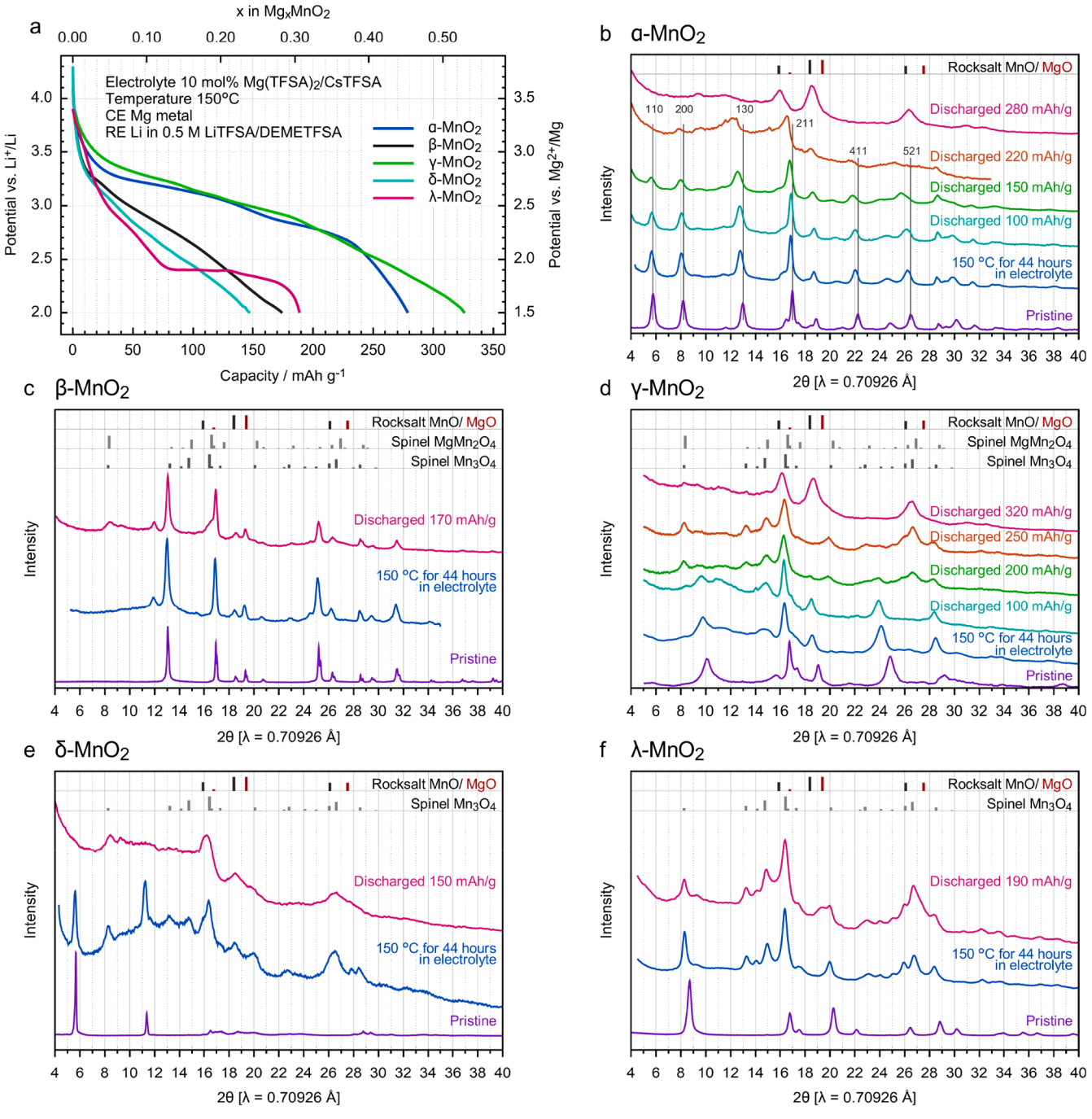

Figure 2. Phase transformations of MnO_2 polymorphs caused by magnesiation at 150 °C. (a) Initial discharge curve of MnO_2 polymorphs in a 10 mol % $Mg(TFSA)_2$/90 mol % CsTFSA electrolyte at a rate of 10 mA/g. (b–f) X ray diffraction patterns of magnesiated α , β , γ , δ , and λ MnO_2. Magnesiation induced phase change was caused by discharge. Spontaneous phase change of unstable MnO_2 polymorphs was caused by isothermal treatment at 150 °C for 44 h in the electrolyte.

leading to reduction of the activation energy of migration and consequently facilitating the Mg migration.[32]

The main peaks of the secondary phase appearing at 8.5° and 16.4° can be assigned to tetragonal spinel Mn_3O_4 with Mg included (*I41/amd*); a deeper degree of magnesiation would be needed to clarify the detailed structure of the secondary phase. Here, it is emphasized that even the most stable β MnO_2 cannot retain its structure, that is, the two phase reaction occurs with Mg insertion.

2.2.3. γ-MnO₂. As seen in Figure 2a, γ MnO_2 *seemingly* exhibits a considerably large discharge capacity of 320 mAh/g (~0.5 Mg per MnO_2) among the MnO_2 polymorphs. However, Figure 2d shows that the magnesiated γ MnO_2 undergoes a two step irreversible phase transformation to spinel $MgMn_2O_4$ (λ $Mg_{0.5}MnO_2$) and eventually rocksalt like $(Mg, Mn)_2O_2$; this is similar to the cases for α MnO_2 and for β MnO_2. Thus, a large degree of magnesiation into MnO_2 polymorphs eventually results in the formation of a spinel type

Table 1. Compositions of MnO_2 Electrodes Discharged in a $Mg(TFSA)_2$/CsTFSA Electrolyte at 150 °C

sample	discharge capacity (mAh/g)	Mg/Mn (based on capacity)[a]	Mg/Mn (ICP)[b]	Li/Mn (ICP)	Cs/Mn (ICP)
α-MnO_2	100	0.16	0.11	<0.015[c]	0.007
α-MnO_2	150	0.24	0.15	<0.012[c]	0.006
α-MnO_2	220	0.36	0.19	<0.014[c]	0.006
α-MnO_2	280	0.45	0.36	<0.013[c]	0.005
β-MnO_2	170	0.28	0.18 (81%)	0.083 (19%)	0.003
γ-MnO_2	100	0.16	0.13	<0.012[c]	0.003
γ-MnO_2	200	0.32	0.22	<0.016[c]	0.005
γ-MnO_2	250	0.41	0.25	<0.012[c]	0.003
γ-MnO_2	320	0.52	0.35 (91%)	0.070 (9%)	0.004
δ-$K_{0.3}MnO_2$	150	0.24	0.15	<0.020[c]	0.012
λ-MnO_2	190	0.31	0.18	<0.027[c]	<0.006[c]

[a]Mg/Mn based on capacity is equal to a discharge capacity divided by a theoretical capacity of 616 mAh/g. [b]The values in parentheses denote the degree of contribution of respective carriers to the capacities. [c]The inequality sign "<" means that the element was not detected; ICP analyses gave the nominal value "< 0.001 mg" for such an element.

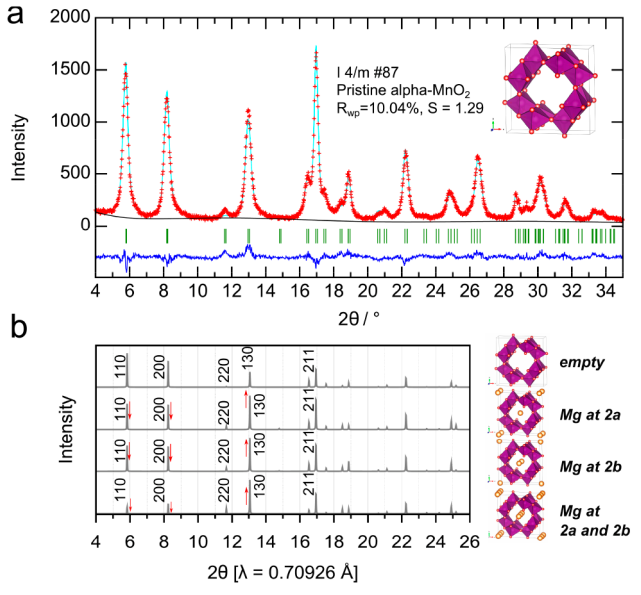

Figure 3. (a) Rietveld refinement of pristine α MnO_2. (b) Simulation of X ray diffraction patterns of α MnO_2 ($I4/m$) with Mg at possible crystallographic sites 2a and 2b. The red arrow shows the change in relative intensity due to the insertion of Mg.

structure and then finally a rocksalt structure, regardless of the initial polymorphic structure of MnO_2.

After being soaked at 150 °C for 44 h in the electrolyte, γ MnO_2 showed only little change in the XRD pattern. Thus, the γ type structure is robust even at elevated temperatures. The XRD pattern of γ MnO_2 can be seen up to 100 mAh/g (~0.16 Mg per MnO_2), suggesting that γ MnO_2 allows topotactic insertion of Mg to some extent. Upon further magnesiation, γ MnO_2 starts to transform to a tetragonal spinel structure before 200 mAh/g (~0.32 Mg per MnO_2) is yielded. The XRD patterns of γ MnO_2 discharged up to 200 mAh/g and 250 mAh/g (0.32 Mg and 0.41 Mg per MnO_2, respectively) are in accord with those of tetragonal spinel structured Mn_3O_4 and $MgMn_2O_4$. After further magnesiation up to 320 mAh/g (0.52 Mg per MnO_2), the XRD patterns eventually are very similar to those of rocksalt MgO and MnO.

Interestingly, the XRD pattern of γ MnO_2 discharged up to 320 mAh/g (0.52 Mg per MnO_2) corresponds to that of a rocksalt like structure. As already stated, this is similar to the case of α MnO_2, in that this discharge capacity is only half (or, for α MnO_2, less than) that required to form rocksalt type MgO + MnO or $MgMnO_2$ (616 mAh/g). As demonstrated in the XRD simulations in Figure 4, the rocksalt like XRD pattern

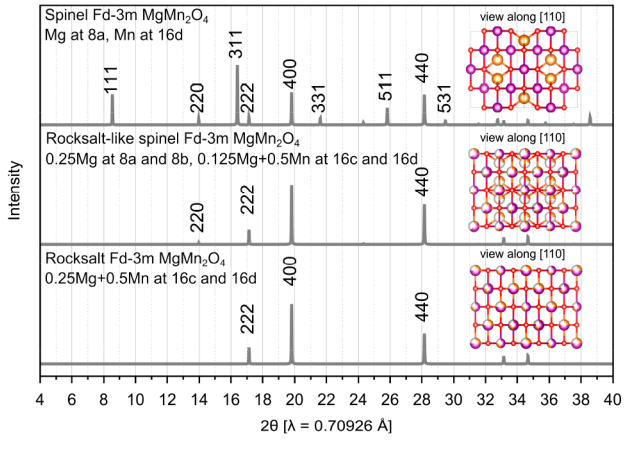

Figure 4. Simulation of X ray diffraction pattern of $Fd3m$ $MgMn_2O_4$ (= $Mg_{0.5}MnO_2$) with a different location of Mg and Mn. 8a and 8b sites correspond to tetrahedral sites while 16d and 16c sites correspond to octahedral sites. The occupation of Mg at 8a (8b) and Mn at 16c (16d) produces a normal spinel structure. Partial disorder between 8a/8b and 16c/16d makes the diffraction pattern similar to that of rocksalt structure.

can be realized, when 16d (octahedral, Mn) and 16c (octahedral, vacancy) sites becomes equivalent by mixing and disordering. Even if some cations partly remain at 8a (tetrahedral, Mg) and/or 8b (tetrahedral, vacancy), namely, even if the structure still has a component of spinel structure, mixing and disordering of 16d and 16c makes the diffraction pattern rocksalt like.

Such an off stoichiometric disordered rocksalt was also observed in our previous study,[33] where a stoichiometric spinel $MgCo_2O_4$ (= $Mg_{0.5}CoO_2$) transforms into a defect rocksalt $Mg_{0.5}CoO_2$ under electron irradiation. The rocksalt like phase shows significantly broad diffraction peaks compared to those of the original α MnO_2 and γ MnO_2 phases. In addition, the lattice constants of the rocksalt like phase (a = 4.41 Å and a = 4.36 Å in the cases of α MnO_2 and γ MnO_2, respectively) estimated from XRD peaks in Figure 2b and d are between those of MgO (a = 4.22 Å) and MnO (a = 4.44 Å). These two characteristics suggest that the rocksalt like phase is substan

tially strained due to the inherent lattice mismatch between the MgO component and MnO component (lattice mismatch of 5.2%, i.e., strain of 2.6%).

It is known that the phase transformation of γ MnO_2 into a spinel structure occurs not only via magnesiation but also via lithiation. According to Thackeray et al.,[34] lithium insertion into γ MnO_2 at 80 °C using mild reducing agent preserves its framework structure up to a composition of $Li_{0.9}MnO_2$. However, an electrochemically lithium inserted γ $Li_{0.5}MnO_2$ readily transforms to the spinel type $LiMn_2O_4$, when being heated to 300 °C. Similarly, magnesiation at 150 °C produces a spinel structure with a composition of $Mg_{0.2-0.4}MnO_2$. These phenomena verify that cation inserted manganese dioxide eventually favors a spinel structure.

2.2.4. δ-MnO_2. Figure 2a lets us assume that δ MnO_2 allows a certain amount of magnesiation, but this is not the case. Actually, δ MnO_2 thermally decomposed into spinel Mn_3O_4 just after being soaked for 44 h in the electrolyte heated to 150 °C (Figure 2e). This spontaneous reduction (oxygen release) at 150 °C indicates that the δ type structure is quite unstable under oxygen free conditions at 150 °C. δ MnO_2 eventually transforms into a rocksalt structure (Mg inserted Mn_3O_4) upon discharge. The magnesiation capacity (150 mAh/g) required to form rocksalt structure is much smaller than that of other polymorphs such as α MnO_2 and γ MnO_2. This is because rocksalt phases can be readily formed from spinel structures via magnesiation; the spinel Mn_3O_4 transforms into rocksalt $MgMn_3O_4$ through a push out process proposed in our previous paper.[5]

In contrast to the present result, several previous works[18,19] have shown excellent reversible Mg aquo ion intercalation/deintercalation cycles in an aqueous electrolyte. It is considered that δ MnO_2 is stabilized at an ambient temperature by the crystal water absorbed inside the structure. In this study, δ MnO_2 was discharged in the full absence of water using ionic liquid electrolyte at an elevated temperature (150 °C). This sharp contrast between aqueous and nonaqueous systems supports crystal water playing a crucial role in reversible insertion/extraction of magnesium and also in stabilization of the δ frame structure, which has been mentioned in the relevant literature.[18,19]

2.2.5. λ-MnO_2. According to the DFT calculation in Figure 8a, λ MnO_2 (i.e., 8a defect spinel structure) is the most unstable at high electrode potentials. As well as δ MnO_2, λ MnO_2 is quite unstable and transforms into spinel Mn_3O_4 by just being soaked in the electrolyte at 150 °C (Figure 2f). This transformation of λ MnO_2 can be explained by a spontaneous reduction with oxygen release in the inner atmosphere. Given that the energy difference between MnO_2 polymorphs is quite small (200 meV in Figure 8a), the chemical driving force of the reduction reaction ($MnO_2 = 1/3Mn_3O_4 + 1/3O_2$) is substantially similar for all of the polymorphs. However, spontaneous reduction was not observed for α MnO_2, β MnO_2, and γ MnO_2. This indicates that the kinetics of spontaneous reduction are considerably fast in λ MnO_2 and δ MnO_2 compared to in the other polymorphs. The spinel Mn_3O_4 formed by the thermal decomposition from λ MnO_2 is further reduced by magnesiation, leading to the formation of a rocksalt phase.

As well as δ MnO_2, the feasibility of magnesium insertion in λ MnO_2 has been reported mainly using aqueous solutions such as a $Mg(NO_3)_2$/water system in several studies.[11−16] In the absence of water, however, it is empirically known that magnesiation capacity is severely limited.[14,35] In this study, we intended to reveal a possible phase transformation path of pure λ MnO_2 in nonaqueous system at elevated temperatures, but this approach was found difficult due to the inherent instability of the λ MnO_2 phase before magnesiation. Although we will discuss this later, this means that the λ MnO_2 phase must be somehow stabilized by a certain treatment, as demonstrated in our previous study[6] ($ZnMnO_3$: ZnO stabilized λ MnO_2), toward practical applications, where the λ MnO_2 phase can hold and magnesiation kinetics are reasonable at elevated temperatures.

2.3. Summary of Phase-Transformation Pathways during Magnesiation at 150 °C. Figure 5 illustrates the transformation pathways of the respective MnO_2 polymorphs experimentally observed in the electrochemical tests done at 150 °C.

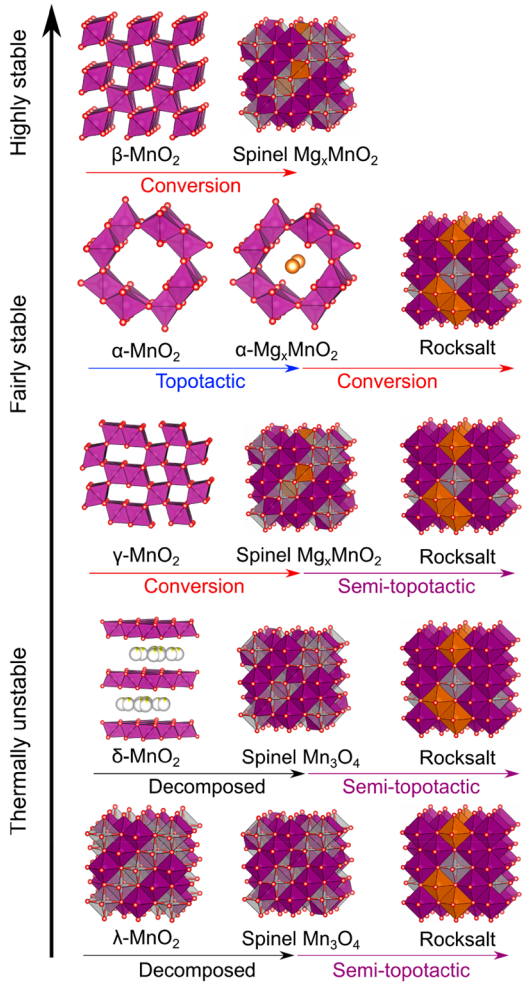

Figure 5. Schematic illustration showing the ergodic pathways of magnesiation induced phase transformation of MnO_2 polymorphs observed experimentally by the electrochemical tests at 150 °C. "Semi topotactic" means that the oxide ion sublattice remains unchanged during the phase transformation between spinel and rocksalt structures.

1. Sufficiently magnesiated α MnO_2 and γ MnO_2 tend to transform to rocksalt type structures without any phase separation. However, the α MnO_2 framework is rather

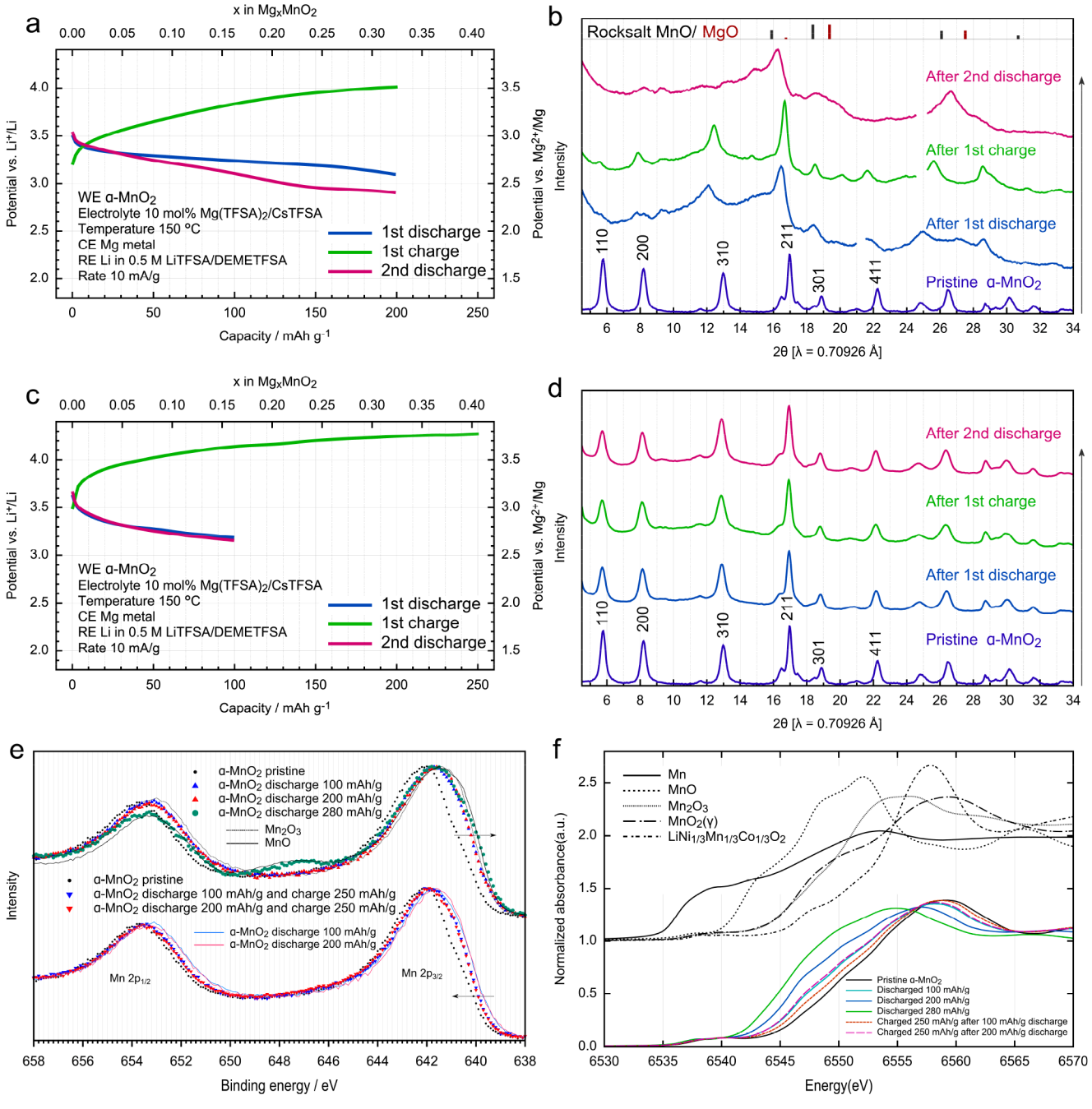

Figure 6. Magnesiation cycles of α MnO_2 in a $Mg(TFSA)_2$/CsTFSA electrolyte at 150 °C. (a) Charge/discharge profiles with a cutoff capacity of 200 mAh/g and (b) corresponding X ray diffraction patterns. (c) Charge/discharge profiles with a cutoff capacity of 100 mAh/g and (d) corresponding X ray diffraction patterns (e, f), X ray photoelectron spectra (XPS), and X ray absorption fine structure (XANES) measured for various magnesiated and demagnesiated α MnO_2.

robust to some extent of magnesiation to allow topotactic insertion.

2. At elevated temperatures, even the most stable β MnO_2 can allow a reaction with Mg to some extent, forming the secondary phase of the spinel structure.

3. In terms of the complete topotactic insertion, the flamework of λ MnO_2 (8a defect spinel type) would be the best structure, but it is the most unstable phase among the polymorphs. In addition, not only λ MnO_2 but also δ MnO_2 is decomposed to spinel type Mn_3O_4, by just being soaked in an electrolyte elevated at 150 °C under oxygen free conditions.

2.4. Reversibility of Mg Intercalation in α-MnO_2. In this section, we focus on the reversibility of intercalation/deintercalation of Mg into/from α MnO_2; see Figure 6. In the charge process, Mg deintercalation from Mg_xMnO_2 is inevitably accompanied by electrolyte oxidation, due to the large overpotentials.[17] Hence, we examined the reversibility of Mg intercalation/deintercalation on α MnO_2 in a few cycles, by using $Mg(TFSA)_2$/CsTFSA ionic liquid that exhibits a wide

electrochemical window.[5] The beaker cell was sufficiently filled with excess electrolyte (6.0 g of electrolyte for 2 mg of α MnO_2) so that the electrochemical cycle can proceed even if the electrolyte is partly oxidized during demagnesiation.

One and half cycles of magnesiation and demagnesiation within a capacity of 200 mAh/g (Figure 6a) already yield a rocksalt structure from α MnO_2 (Figure 6b). After the first magnesiation of 200 mAh/g, the α type structure is still observed in the diffraction pattern, although the broad diffraction peaks imply that the magnesiated α type structure was distorted. The crystallinity of α MnO_2 is then recovered by charging up to 200 mAh/g. While the slight peak shift toward higher angles implies that magnesium is extracted from α MnO_2, the crystal structure does not completely revert to the pristine state by charging, suggesting an incomplete extraction of inserted magnesium. Because the colorless electrolyte turned to light brown during charging, incomplete magnesium removal can be attributed to the oxidation of electrolytes competing with demagnesiation. Due to such an incomplete removal of Mg, the second magnesiation of 200 mAh/g leads to overmagnesiation and transformation of the α type structure into rocksalt structure.

To demonstrate a reversible magnesiation of α MnO_2, the discharge capacity was limited to 100 mAh/g. Since the charge capacity inevitably involves electrolyte oxidation during the demagnesiation process, the subsequent charge was excessively extended up to 250 mAh/g (Figure 6c) to completely extract the magnesium ions. As a consequence of excess charge and limited discharge, the α type structure is successfully preserved during one and half cycles (Figure 6d).

The fact that α type structure is maintained even after the second discharge of 100 mAh/g indicates that the inserted Mg ions are extracted by the excess charge. These results show that α MnO_2 allows reversible magnesiation under the following conditions: (i) limited discharge and (ii) overcharge. When magnesiation capacity reaches 200 mAh/g, the crystallinity of α MnO_2 is significantly lowered. Therefore, the limitation of discharge capacity can contribute to the reversible magnesiation/demagnesiation processes. Demagnesiation from α MnO_2 inevitably accompanies oxidation of electrolyte even in TFSA based ionic liquid that shows an excellent resistance to oxidation. Efficient demagnesiation from α MnO_2 could possibly be achieved with advanced electrolytes with higher oxidation stability.

The reversibility of magnesium intercalation in α MnO_2 was also investigated in terms of the valence state of Mn using X ray photoelectron spectroscopy (XPS). The Mn $2p_{3/2}$ spectrum gradually shifts to lower binding energy by discharging pristine α MnO_2; see Figure 6e (upper spectra). The spectra after topotactic magnesium insertion up to 100 mAh/g and 200 mAh/g are located between those of pristine α MnO_2 (Mn^{4+}) and Mn_2O_3 (Mn^{3+}), indicating the gradual reduction of Mn^{4+} toward Mn^{3+}. Interestingly, magnesiation up to 280 mAh/g to form a rocksalt phase yields a satellite peak appearing at 647.5 eV, which suggests the presence of Mn^{2+} in the rocksalt like phase. Since the discharge amount of 280 mAh/g corresponds to a valence change of only 0.91 (i.e., Mn^{4+} to $Mn^{+3.09}$), it can be considered that Mn^{2+} appears via disproportionation reaction of Mn^{3+} into Mn^{2+} and Mn^{4+}. This hypothesis also rationalizes the fact that the rocksalt like phase does not exhibit Jahn–Teller distortion unlike typical Mn^{3+} compounds such as tetragonal spinel $MgMn_2O_4$.

Furthermore, the demagnesiated states from the magnesiated α (Mg)MnO_2 were also investigated by sufficiently charging up to 250 mAh/g (including a competing electrolyte decomposition) after discharging 100 mAh/g and 200 mAh/g; Figure 6e (lower spectra). The Mn $2p_{3/2}$ spectrum gradually shifts to higher energy upon charging. This indicates the reversible oxidation of Mn via demagnesiation reaction. The corresponding decrease in the magnesium composition was also confirmed by energy dispersive X ray (EDX) spectroscopy (see Figure S8). Nevertheless, it should be noted that the Mn $2p_{3/2}$ spectra do not completely revert back to the pristine state (Mn^{4+}), which is probably due to the limited electrochemical window of the electrolyte.

Moreover, to obtain the bulk sample information on the valence change of Mn before/after magnesiation and demagnesiation, X ray absorption near edge structure (XANES) measurements have been performed at BL14B2, SPring 8. Figure 6f shows the XANES spectra near the Mn K edge energy with several reference spectra of the typical manganese oxides and Mn metal. After discharge (magnesiation of 100, 200, 280 mAh/g), each K edge profile shifts to lower energy, while the edge reverts to the higher energy side after charge (demagnesiation of 250 mAh/g after magnesiation of 100 and 200 mAh/g). As well as the XPS results, after magnesiation of 280 mAh/g, the K edge profile partially resembles the MnO spectrum, which means that the divalent Mn exists inside the bulk sample, even far below the rocksalt composition, which is corroborated by the XRD profile in Figure 2b. Thus, the tendency of the valence change measured by XANES is in very good agreement with the surface information on the Mn valence change by XPS.

To demonstrate the cyclability, a prolonged cycle test was performed in a more limited capacity condition. In this experiment, to compensate for the low efficiency of the demagnesiation reaction due to the competing electrolyte oxidation that can occur above about 4 V vs Li^+/Li, the charge process was extended to 150 mAh/g, which is larger than the discharge capacity of 80 mAh/g. The cycle reversibility of magnesiation and demagnesiation is shown in Figure 7 (see also Figure S9 for XRD profile after the cycle test), which indicates that α MnO_2 is capable of exerting over 10 cycles of topotactic magnesiation and demagnesiation at an elevated

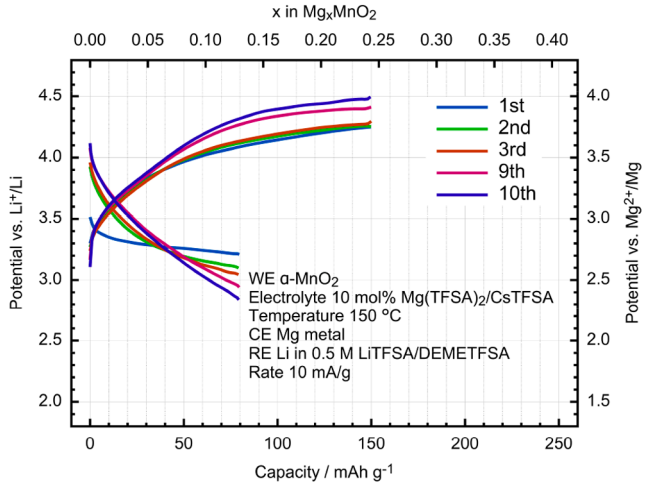

Figure 7. Cycle test of α MnO_2 at 150 °C under limited capacity conditions: 80 mAh/g discharge and 150 mAh/g charge.

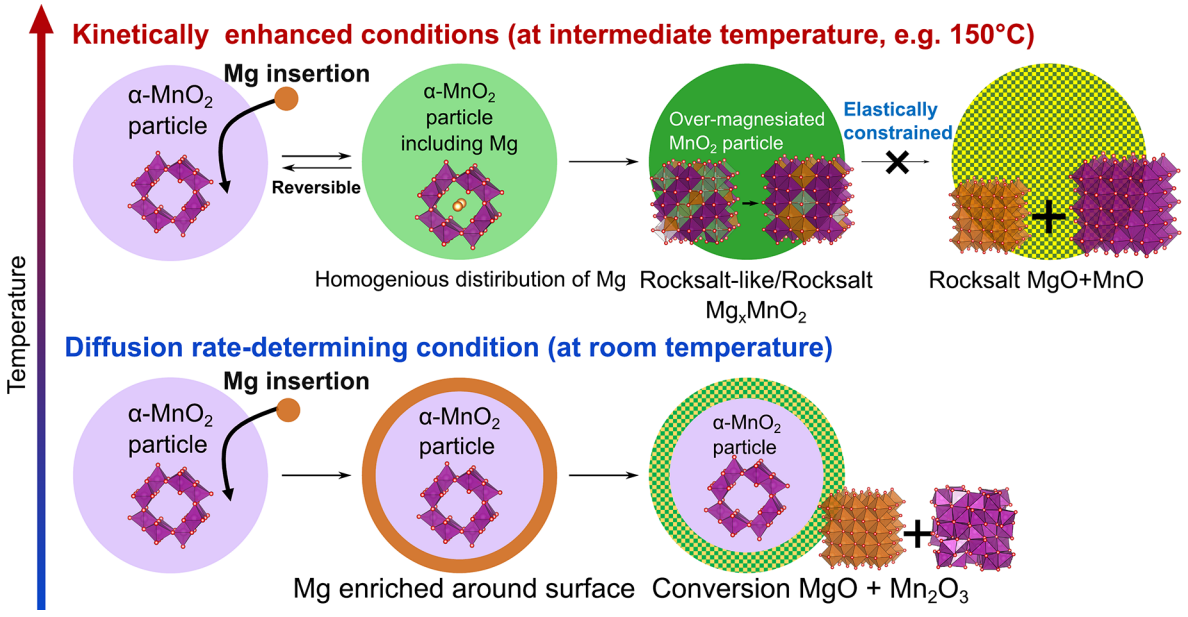

Figure 8. Schematic illustration showing the two kinds of magnesiation pathways of α MnO_2 particles at intermediate temperature and room temperature, where the latter pathway was based on the previous work by Arthur et al.[25]

temperature (150 °C) under conditions of a limited discharge capacity of 80 mAh/g.

Figure 8 illustrates two kinds of magnesiation pathways for α MnO_2 with or without elevating the operating temperature. The previous works on α MnO_2 have reported that electro chemical magnesiation of α MnO_2 at room temperature results in a conversion reaction to form amorphous like (Mg, Mn)O on/around the surface of active material.[24,25] Similarly, the present magnesiation experiment at 150 °C also demonstrated the formation of a rocksalt like phase from α MnO_2 after magnesiation up to 280 mAh/g (Figure 2a). Nevertheless, our experiment at 150 °C clearly demonstrates a topotactic intercalation of Mg ions in α MnO_2 to form the solid solution region within a limited range of magnesium composition (x < 0.3 in Mg_xMnO_2) and prolonged electrochemical cycling. This difference implies that sluggish Mg kinetics at room temper ature enrich magnesium around or at the surface of active material, resulting in the occurrence of a local conversion reaction. Thus, the topotactic magnesiation at 150 °C implies that the conversion reaction can be avoided by enhancing the kinetics of Mg intercalation. Namely, enhanced migration kinetics of magnesiation can alleviate overmagnesiation around the surface that leads to the formation of conversion products such as rocksalt phases. As discussed in the next section, also in a further magnesiation from the rocksalt like phase, the phase separation, MgO + MnO (both are rocksalt type), is unlikely in that the coherent strain energy would exceed the chemical driving force of the phase separation.

3. DISCUSSION

In this section, we shall discuss the thermodynamic validity of these pathways in Figure 5. Using DFT calculations, we calculated the formation energies of the following five kinds of MnO_2 polymorphs: α, β, R, δ, and λ. In addition, following the approach by Ling et al.,[26] the formation energies of possible decomposition products (such as rocksalt MgO + bixbyite Mn_2O_3, rocksalt MgO + spinel Mn_3O_4, rocksalt MgO + rocksalt MnO) were calculated to compare with those of magnesiated MnO_2 polymorphs. Based on the reaction of hcp Mg metal and λ MnO_2 that is the most unstable structure between the polymorphs[36] (as demonstrated in the present experiments, Figure 2), the formation energies of respective magnesiated polymorphs Mg_xMnO_2 at 0 K were obtained by the following equation:

$$\Delta E_{Mg_xMnO_2} = E_{Mg_xMnO_2} - (xE_{Mg} + E_{\lambda-MnO_2})$$

where $\Delta E_{Mg_xMnO_2}$ denotes the formation energy of Mg_xMnO_2 and $E_{Mg_xMnO_2}$, $E_{\lambda-MnO_2}$, and E_{Mg} represent the internal energies of the respective compounds. The detailed calculation procedure for the structure determination is described in the Supporting Information (Figure S10).

Figure 9a (upper) shows the formation energy $\Delta E_{Mg_xMnO_2}$ as a function of the Mg composition x and also shows the energy gain by the phase decomposition with magnesiation. A typical plausible structure at each composition of Mg for each polymorph is also displayed in Figure 9a, which was obtained after relaxation from each initial structure (by a local minimum convergence without drastic structure change). Figure 9a (lower) gives the electrode potential versus Mg from the calculated formation energy. Since we suppose that the negative electrode is Mg metal, the voltage for Mg_xMnO_2 + ΔxMg = $Mg_{x+\Delta x}MnO_2$ is given by $V = -(\Delta E_{Mg_{x+\Delta x}MnO_2} - \Delta E_{Mg_xMnO_2})/2\Delta x$.

It is indicated that possible magnesiated products are λ $Mg_{0.5}MnO_2$ (spinel $MgMn_2O_4$), spinel Mn_3O_4 + rocksalt MgO, rocksalt MgO + rocksalt MnO, and rocksalt $MgMnO_2$. What is the most important here is that, between x = 0 and 0.5 in Mg_xMnO_2, the ground state energy is attained for the two phase state of each polymorph MnO_2 + λ $Mg_{0.5}MnO_2$. The lowest formation energy for λ $Mg_{0.5}MnO_2$ at x = 0.5 excludes the possibility of the conversion reaction, λ MnO_2 + 1/2Mg = 1/2MgO (rocksalt) + 1/2Mn_2O_3 (bixbyite). This is also corroborated by the fact that the spinel type $MgMn_2O_4$ is also a stable natural mineral. Namely, the magnesiated MnO_2 polymorphs (α, β, R, and δ MnO_2) other than λ MnO_2

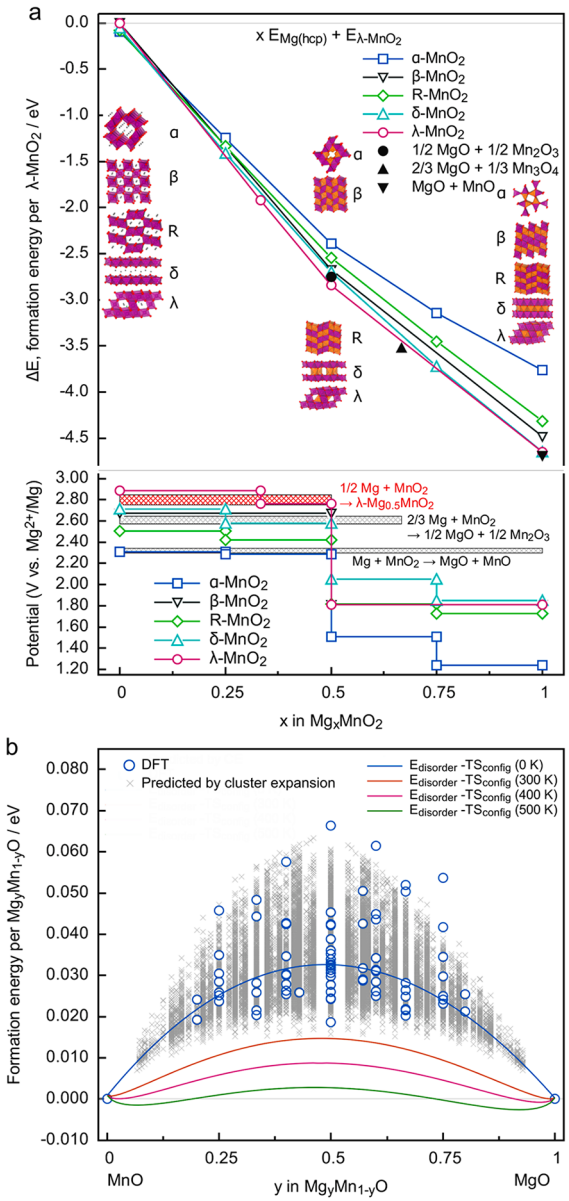

Figure 9. (a) Upper: Formation energies of magnesiated MnO_2 polymorphs and possible decomposition products based on DFT calculation. The convex ground state hull of each polymorph was determined by calculating more than 100 possible Mg Va configurations (see Figure S7). The formation energies are shown with respect to energies of xMg and λ MnO_2. The energies are given by the relaxed structures shown in the figure. Purple, orange, and red atoms represent Mn, Mg, and O, respectively. Possible Mg sites are shown as black dots in the structures at x = 0.0. (a) Lower: Computed voltage of magnesiation at 0 K as a function of Mg concentration. Red shadow area indicates the potential range upon magnesiation that transforms each MnO_2 phase (α, β, γ, δ, or λ) into λ $Mg_{0.5}MnO_2$ (stoichiometric spinel $MgMn_2O_4$) through 1/2Mg + MnO_2 (α, β, γ, δ, or λ) → λ $Mg_{0.5}MnO_2$. Black shadow area shows the potential range of conversion reaction of original MnO_2 polymorphic structures into Mn_2O_3 and MnO. The voltage of the conversion reactions varies within 0.1 V depending on MnO_2 structures. (b) Formation energies of disordered rocksalt $Mg_yMn_{1-y}O$ in comparison to two phase separation into yMgO + $(1 - y)$MnO.

would eventually transform to the most stable spinel type λ $Mg_{0.5}MnO_2$ after magnesiation, provided that the magnesium diffusion is sufficiently active. Especially, α Mg_xMnO_2 is suggested from Figure 9a to be a less stable structure than other magnesiated polymorphs. Therefore, it deserves to be noted that the experimentally observed topotactic insertion in α Mg_xMnO_2 (as shown in Figures 2b and 6) can take place while being retained metastably. That is, the substantial instability of α Mg_xMnO_2 suggests that the topotactic pathway would inexorably disappear when thermodynamic equilibration is indeed achieved (probably, at much higher temperatures). Thus, the gradual structural breakdown into the spinel/rocksalt phase could be another factor that promotes irreversible cycling as well as electrolyte decomposition.

From the viewpoint of the DFT calculation, λ MnO_2 (also δ MnO_2 and R MnO_2) can topotactically accommodate Mg up to x = 1, whereas α MnO_2 and β MnO_2 undergo a nontopotactical structure change before x reaches 1. Therefore, the λ MnO_2 framework is the best structure in terms of complete topotactic Mg insertion. However, practically λ MnO_2 (and also δ MnO_2) cannot retain its host structure at elevated temperatures, e.g., 150 °C. Therefore, it is necessary to consider how to enhance the thermal stability for the two polymorphs. A plausible solution is $ZnMnO_3$, which is stabilized by mixing ZnO with λ MnO_2.[6]

Although we experimentally observed no further magnesiation process in this work, we discuss the transformation behavior based on the results of the DFT calculation. At x = 0.66, the two phase state, 2/3MgO (rocksalt) + $1/3Mn_3O_4$ (spinel), is in the lowest formation energy state; namely, even the most stable λ $Mg_{0.5}MnO_2$ could also be decomposed to these phases. In practice, however, unless the operation temperature is raised, this phase decomposition from λ $Mg_{0.5}MnO_2$ once formed would be kinetically hindered at low temperatures due to slow migration kinetics of Mg and Mn polyvalent cations.

At x = 1.0, although the ground state is a two phase state of MgO (rocksalt) + MnO (rocksalt), a tentative ordered rocksalt structure of $MgMnO_2$ occupied with Mg at 16c and Mn at 16d sites in $Fd3m$ also shows a quite close formation energy (only 18.5 meV per $Mg_{0.5}Mn_{0.5}O$ higher in Figure 9a). Such close formation energies of $MgMnO_2$ and MgO + MnO imply that mixed Mg−Mn configurations in the cation sublattice of the rocksalt structure with the fixed fcc oxygen sublattice are achieved by small excess energies.

For a more accurate analysis, we also considered the mixing entropy effects on the phase stability of these phases. Figure 9b shows the free energy of the quasi binary system of MgO and MnO at various temperatures. The formation energy of disordered rocksalt $Mg_yMn_{1-y}O$ was estimated by the cluster expansion method; the validity of the evaluation is supported by the formation energies substantially equaling zero at y = 0 and y = 1. The blue curve in Figure 9b indicates that the disordered rocksalt at y = 0.5 yields an excess of only 32 meV per $Mg_{0.5}Mn_{0.5}O$ from the ground state 1/2(MgO + MnO). Since this excess energy (32 meV/$Mg_{0.5}Mn_{0.5}O$) is comparable to the mixing entropy TS_{mix} = RT ln 2 (e.g., 25 meV/$Mg_{0.5}Mn_{0.5}O$ at 150 °C), the disordered single phase $Mg_{0.5}Mn_{0.5}O$ is likely to appear as well as the separated state, 0.5MgO + 0.5MnO. In addition, this phase separation may further be prevented due to a large lattice mismatch between MgO and MnO (ca. 5.2%); the phase separation requires additional 50−60 meV (/$Mg_{0.5}Mn_{0.5}O$) as a coherent strain energy (given that the bulk modulus is about 150 GPa).[37−39] Actually, we have observed in our previous studies[5,17] that Mg

insertion into spinel λ $Mg_{0.5}MnO_2$ forms a single phase disordered rocksalt $MgMnO_2$ (= $Mg_{0.5}Mn_{0.5}O$). Also, in the rocksalt like phases observed (even far below the rocksalt composition) in α MnO_2 and γ MnO_2, the same argument would be applied; the phase separation would be retarded or hindered as shown in Figure 8.

The calculated electrode potentials upon magnesiation of MnO_2 at 0 K are shown in Figure 9a (lower). The electrode potential of magnesiation that transforms MnO_2 polymorphs into λ $Mg_{0.5}MnO_2$ is around 2.8 V vs Mg^{2+}/Mg, being in agreement with our previous work.[5] This voltage is the highest among those for the topotactic magnesiation in α, β, δ, and R MnO_2, suggesting that a transformation to λ $Mg_{0.5}MnO_2$ from each magnesiated polymorph other than λ MnO_2 is thermodynamically favorable compared to the topotactic magnesiation for α, β, δ, and R MnO_2. Another conversion reaction to form 2/3MgO + 1/3Mn_3O_4 (spinel) also shows a higher voltage than that of the topotactic magnesiation reaction of α MnO_2 (and also R MnO_2), being consistent with the argument pointed out in the previous works.[25−27] This indicates that the former is likely in thermodynamics, and therefore, the topotactic reactions in α MnO_2 and R MnO_2 actually observed would occur "metastably".

In terms of the high electrode potential and structure similarity before/after magnesiation, future research should aim to somehow stabilize λ MnO_2 in order to obtain the best cathode performance. In contrast to the excellent phase stability of spinel $MgMn_2O_4$, the instability of the λ MnO_2 phase hinders stable magnesiation cycling, especially at elevated temperatures. However, we substantiated that, for the topotactic magnesiation of metastable α MnO_2, the host framework does not always necessarily need to be thermodynamically stable but needs to be kinetically stable enough against irreversible phase transformations. On the basis of this recipe, it would be justified to find out certain chemical elements that kinetically prevent irreversible phase transformation of λ MnO_2. Our recent work clearly demonstrated that chemical doping of Zn significantly stabilizes the defect spinel structure,[6] but this approach still needs further optimization in terms of capacity as a future work.

Finally, we remark on the enhancement of the magnesium insertion kinetics into MnO_2 polymorphs, which would be improved by controlling the crystal facets and surfaces of the active materials. As well as magnesium migration in an oxide framework, the desolvation process on the surface of the cathode materials seemingly limits the rate of magnesium insertion. Recently, Prendergast et al. suggested that desolvation kinetics of the magnesium complex ($Mg\ TFSA^+$ and $Mg-Cl^+$) on oxide cathodes is highly facilitated on a certain crystal facet of the cathode material (e.g., MoO_3).[40,41] They also established the advanced molecular dynamics free energy sampling technique that enables the prediction of the solvation structures of polyvalent cations having multiple stable structures.[40] This technique would be helpful for modification of MnO_2 cathodes and a search for compatible electrolytes.

4. CONCLUSIONS

This study has investigated the behavior of the magnesiation induced transformations of five MnO_2 polymorphs at an intermediate temperature. The polymorphs α, β, γ (R), δ, and λ type MnO_2 were electrochemically magnesiated at 150 °C, and their phase transformations were experimentally analyzed and interpreted in the light of the prediction of the ab initio calculation in density functional theory (DFT). The accelerated electrochemical tests have clearly indicated that there is a strong tendency for all the MnO_2 polymorphs to transform into spinel and then rocksalt phases upon magnesiation and/or thermal decomposition. It has been shown that only α MnO_2 is kinetically stable in terms of resistance against the spinel and/or rocksalt transformations and allows a significant Mg intercalation and deintercalation with no change of the framework.

The salient results can be summarized as follows:

(1) Although α MnO_2 eventually transforms into rocksalt when the discharge capacity reaches 270 mAh/g, α MnO_2 can allow Mg intercalation up to 150−220 mAh/g without transformations into spinel and rocksalt phases.

(2) Mg insertion into β MnO_2 was demonstrated for the first time. Even the most stable polymorph β MnO_2 can allow a reaction with Mg to some extent at elevated temperatures. β MnO_2 would eventually transform to a spinel/rocksalt structure.

(3) γ MnO_2 consisting of R type and β type structures exhibits a high discharge capacity over 300 mAh/g, but this large capacity is attributed to an irreversible reaction, that is, transformation of the original framework γ MnO_2 into spinel and eventually rocksalt phases.

(4) The fact that λ MnO_2 and δ MnO_2 are thermally decomposed to the spinel Mn_3O_4 by being soaked in an electrolyte at 150 °C (without any electrochemical reactions) indicates that their structure stabilities are quite poor among the MnO_2 polymorphs. In contrast, it should be noted that the magnesiated λ MnO_2 (i.e., spinel $MgMn_2O_4$) is the thermodynamically most stable phase.

(5) Thus, only α type structure can resist the strong driving force of the magnesiation induced transformation to spinel structure and subsequent rocksalt structure, especially at elevated temperatures.

(6) As indicated by the ab initio calculations, the conversion route to form spinel/rocksalt phases is thermodynamically more favorable than the topotactic intercalation even in α MnO_2. Therefore, the experimental fact that α MnO_2 allows Mg intercalation to a large extent, indicates that the α MnO_2 framework can be kinetically retained, and Mg intercalation is faster than conversion reactions in the α type structure.

(7) Although α MnO_2 yields a topotactic magnesiation capacity of about 200 mAh/g in the initial discharge, subsequent electrochemical cycling of 200 mAh/g eventually leads to forming rocksalt structure. This is because extraction of Mg in the charge process was insufficient within the electrochemical window of the ionic liquid. However, it was found that α MnO_2 can allow reversible magnesium intercalation/deintercalation at a certain limited capacity (e.g., 100 mAh/g). α MnO_2 needs to be carefully designed as a cathode material for RMBs, because irreversible phase changes take place when it is overdischarged.

(8) From theoretical viewpoints, λ MnO_2 is expected to exhibit high magnesiation capacity through complete topotactic insertion of Mg without any change of its framework. Because λ MnO_2, spinel λ $Mg_{0.5}MnO_2$, and rocksalt $MgMnO_2$ share the common anion sublattice, λ MnO_2 is expected to undergo coherent phase transformation over a wide range of Mg compositions. It would therefore be a key challenge to consider how to stabilize λ MnO_2 that is unstable compared to other MnO_2 polymorphs.

5. METHODS

5.1. Experimental Method. α MnO_2 and β MnO_2 were produced by hydrothermal synthesis methods reported by Wang et al.[42] For the synthesis of α MnO_2, oxidizing agents, $(NH_4)_2S_2O_8$, and NH_4SO_4 were dissolved into a 0.67 mol/L $MnSO_4$ aqueous solution at a molar ratio of $MnSO_4/(NH_4)_2S_2O_8/NH_4SO_4$ = 1.0:1.0:1.875. The solution was transferred into a Teflon lined stainless steel autoclave and heated at 140 °C for 12 h. For the synthesis of β MnO_2, $(NH_4)_2S_2O_8$ was dissolved into an aqueous solution of 1.0 mol/L $MnSO_4$ mixed at a molar ratio of $MnSO_4/(NH_4)_2S_2O_8$ = 1.0:1.0 and heated within a Teflon lined stainless steel autoclave at 180 °C for 6 h. Similarly, for γ MnO_2, $(NH_4)_2S_2O_8$ was dissolved into 0.25 mol/L $MnSO_4$ aqueous solution at a molar ratio of $MnSO_4/(NH_4)_2S_2O_8$ = 1.0:1.0, and the resulting solution was heated in a Teflon lined stainless steel autoclave at 60 °C for 12 h.

λ MnO_2 was produced by chemically extracting Li from spinel $LiMn_2O_4$. Spinel $LiMn_2O_4$ was prepared from α MnO_2 and LiOH by heating the stoichiometric mixture at 480 °C for 10 h. The $LiMn_2O_4$ powder was immersed in 0.4 M HCl aqueous solution to extract Li. The powder was filtered and washed with distilled water several times followed by vacuum drying.

δ MnO_2 was prepared following Gaillot et al.[43] $KMnO_4$ crystalline powder was thermally decomposed at 700 °C in air. In order to remove soluble byproducts, the powder was washed with distilled water several times until a colorless solution was obtained. The remaining insoluble black powder was filtered and dried in a vacuum at 80 °C.

MnO_2 electrodes were prepared by coating a slurry of 80 wt % MnO_2, 10 wt % carbon black, and 10 wt % polyvinylidene difluoride dispersed in *N* methylpyrrolidone (NMP) on Al foil. The coated electrodes were then dried at 50−120 °C in a vacuum for 12 h. The loading of MnO_2 on the electrode was 1.2−2.2 mg/cm^2.

Electrochemical measurements were performed using a three electrode beaker cell in an Ar filled glovebox. The beaker was filled with 6.0 g of electrolyte composed of 10 mol % $Mg(TFSA)_2$ ("TFSA" represents $(CF_3SO_2)_2N$ anion/bis(trifluoromethanesulfonyl)amide) and 90 mol % CsTFSA. This ionic liquid electrolyte has good thermal stability at 150 °C during the measurement.[44,45] The addition of CsTFSA to $Mg(TFSA)_2$ allows adjustment of the melting temperature of the binary ionic liquid. CsTFSA exhibits a lower melting temperature (120 °C) than other TFSA salts. Because the melting temperature of pure $Mg(TFSA)_2$ is too high for using Li metal as a reference electrode (the melting point of Li metal is 180 °C), the melting temperature of the binary ionic liquid was adjusted to be below 120 °C at a molar ratio of 90% CsTFSA/10% $Mg(TFSA)_2$.[46,47]

A Mg metal ribbon was used as the counter electrode. A glass tube Li reference electrode used in the beaker cell was prepared by immersing Li foil into 0.1 M LiTFSA/N,N diethyl *N* methyl N (2 methoxyethyl)ammonium bis(trifluoro methanesulfonyl)amide (DEMETFSA). The reference electrode was electrically connected to the $Mg(TFSA)_2$/CsTFSA electrolyte with a liquid junction of a porous ceramic filter. The cyclic voltammetry measurements were performed at a scan rate of 1 mV/s. Mangnesiation induced phase change was caused by galvanostatic discharge performed at a rate of 10 mA/g in the electrolyte at 150 °C. Spontaneous phase change of unstable MnO_2 polymorphs was induced by isothermal treatment at 150 °C for 44 h in the electrolyte. Electrochemical data were collected using a VMP3 potentiostat/galvanostat (Bio Logic SAS). The MnO_2 electrodes were immersed in acetonitrile to remove the remaining electrolyte before characterization.

The prepared MnO_2 powders were characterized with a field emission scanning electron microscope (FE SEM, JEOL, JSM 7200F) operating at an accelerating voltage of 5 kV.

X ray powder diffraction (XRD) analysis was performed using a Rigaku SmartLab diffractometer with Mo Ka radiation (λ = 0.70926 Å). The pristine powders were characterized with Bragg−Brentano geometry, and the electrode materials upon electrocehical treatment were characterized with Debye−Scherrer geometry after being sealed in a Lindeman glass capillary. The experimental diffraction patterns were compared to the simulation results calculated by the VESTA program.[48] Simulation of XRD patterns of γ MnO_2 was performed with the DIFFaX program[49] following Chabre et al.[29]

XPS measurements were performed using an X ray photoelectron spectrometer (Fisons Instruments, S probe) for the electrode samples, and XANES measurements were conducted for the pelletized samples with BN powders at BL14B2, SPring 8.

5.2. Computational Method. The density functional theory (DFT) calculations were implemented with Projector Augmented Wave (PAW)[50] potentials using Vienna *Ab initio* Software Package (VASP).[51,52] The exchange correlation effects were described with Perdew−Burke−Ernzerhof (PBE) generalized gradient approximation (GGA).[53] The plane wave cutoff energy was set at 520 eV. To obtain formation energies close to the experimental values in a wide range of Mn oxidation states, on site Coulomb interactions were corrected with the Hubbard U parameter of 3.9 eV following the literature.[54,36] We relaxed ionic positions, lattice parameters, and angles until the energy converged to less than 10^{-4} eV per MnO_2. The atom configurations were relaxed according to the conjugate gradient method. Although the formation energies of MnO_2 depend on the magnetic structures, we confirmed that the energies vary within 0.05 eV per MnO_2 of all polymorphs by calculating more than 20 possible magnetic structures. A possible Mg Va configuration of Mg_xMnO_2 was produced using the Alloy Theoretic Automated Toolkit (ATAT).[55,56] The crystal structures were visualized using the VESTA program.[48]

AUTHOR INFORMATION

Corresponding Authors

Takuya Hatakeyama − *Institute for Materials Research, Tohoku University, Sendai 980 8577, Japan; Graduate School of Engineering, Tohoku University, Sendai 980 8579, Japan;* orcid.org/0000 0003 4593 5929; Email: hatakeyama t@imr.tohoku.ac.jp

Tetsu Ichitsubo − *Institute for Materials Research, Tohoku University, Sendai 980 8577, Japan;* orcid.org/0000 0002 1127 3034; Email: tichi@imr.tohoku.ac.jp

Authors

Hongyi Li − *Institute for Materials Research, Tohoku University, Sendai 980 8577, Japan;* orcid.org/0000 0003 1890 3825

Norihiko L. Okamoto − *Institute for Materials Research, Tohoku University, Sendai 980 8577, Japan;* orcid.org/0000 0003 0199 7271

Kohei Shimokawa − *Institute for Materials Research, Tohoku University, Sendai 980 8577, Japan;* orcid.org/0000 0003 3261 9679

Tomoya Kawaguchi − *Institute for Materials Research, Tohoku University, Sendai 980 8577, Japan;* orcid.org/0000 0002 7600 4847

Hiroshi Tanimura − *Institute for Materials Research, Tohoku University, Sendai 980 8577, Japan*
Susumu Imashuku − *Institute for Materials Research, Tohoku University, Sendai 980 8577, Japan;* orcid.org/0000 0001 8464 2980
Maximilian Fichtner − *Helmholtz Institute Ulm (HIU) Electrochemical Energy Storage, 89081 Ulm, Germany; Institute of Nanotechnology, Karlsruhe Institute of Technology, D 76021 Karlsruhe, Germany*

Notes

The authors declare no competing financial interest.

■ ACKNOWLEDGMENTS

We are indebted to K. Nakayama and Y. Kabasawa in the Analytical Research Core for Advanced Materials, IMR, Tohoku University for their help in the ICP analyses. The authors acknowledge funding support from the Advanced Low Carbon Technology Research and Development Program (ALCA, grant number: JPMJAL1301). The authors acknowl edge the Center for Computational Materials Science, Institute for Materials Research, Tohoku University for the use of MASAMUNE IMR (project no. 20S0401, 20S0405). One of the authors, T.H., acknowledges support from the Graduate Program in Materials Science at Tohoku University. M.F. acknowledges funding from the German Research Foundation (DFG) under Project ID 390874152 (POLiS Post Lithium Storage Cluster of Excellence). The work also contributes to the research performed at CELEST (Center for Electro chemical Energy Storage Ulm Karlsruhe).

■ REFERENCES

(1) Gregory, T. D.; Hoffman, R. J.; Winterton, R. C. Applications to Energy Storage Nonaqueous Electrochemistry of Magnesium : Service Email Alerting. *J. Electrochem. Soc.* **1990**, *137*, 775−780.
(2) Aurbach, D.; Lu, Z.; Schechter, A.; Gofer, Y.; Gizbar, H.; Turgeman, R.; Cohen, Y.; Moshkovich, M.; Levi, E. Prototype Systems for Rechargeable Magnesium Batteries. *Nature* **2000**, *407*, 724−727.
(3) Yoo, H. D.; Shterenberg, I.; Gofer, Y.; Gershinsky, G.; Pour, N.; Aurbach, D. Mg Rechargeable Batteries: An on Going Challenge. *Energy Environ. Sci.* **2013**, *6*, 2265.
(4) Matsui, M. Study on Electrochemically Deposited Mg Metal. *J. Power Sources* **2011**, *196*, 7048−7055.
(5) Okamoto, S.; Ichitsubo, T.; Kawaguchi, T.; Kumagai, Y.; Oba, F.; Yagi, S.; Shimokawa, K.; Goto, N.; Doi, T.; Matsubara, E. Intercalation and Push Out Process with Spinel to Rocksalt Tran sition on Mg Insertion into Spinel Oxides in Magnesium Batteries. *Advanced Science* **2015**, *2*, 1500072.
(6) Shimokawa, K.; Atsumi, T.; Okamoto, N. L.; Kawaguchi, T.; Imashuku, S.; Wagatsuma, K.; Nakayama, M.; Kanamura, K.; Ichitsubo, T. Structure Design of Long Life Spinel Oxide Cathode Materials for Magnesium Rechargeable Batteries. *Adv. Mater.* **2021**, *33*, 2007539.
(7) Thackeray, M. M. Manganese Oxides for Lithium Batteries. *Prog. Solid State Chem.* **1997**, *25*, 1−71.
(8) Ohzuku, T.; Kitagawa, M.; Hirai, T. Electrochemistry of Manganese Dioxide in Lithium Nonaqueous Cell. *J. Electrochem. Soc.* **1990**, *137*, 769.
(9) Thackeray, M. M.; David, W. I. F.; Bruce, P. G.; Goodenough, J. B. LITHIUM INSERTION INTO MANGANESE SPINELS. *Mater. Res. Bull.* **1983**, *18*, 461−472.
(10) Feng, Z.; Chen, X.; Qiao, L.; Lipson, A. L.; Fister, T. T.; Zeng, L.; Kim, C.; Yi, T.; Sa, N.; Proffit, D. L.; Burrell, A. K.; Cabana, J.; Ingram, B. J.; Biegalski, M. D.; Bedzyk, M. J.; Fenter, P. Phase Controlled Electrochemical Activity of Epitaxial Mg Spinel Thin Films. *ACS Appl. Mater. Interfaces* **2015**, *7*, 28438−28443.
(11) Cabello, M.; Alcántara, R.; Nacimiento, F.; Ortiz, G.; Lavela, P.; Tirado, J. L. Electrochemical and Chemical Insertion/Deinsertion of Magnesium in Spinel Type MgMn2O4 and Lambda MnO2 for Both Aqueous and Non Aqueous Magnesium Ion Batteries. *CrystEngComm* **2015**, *17*, 8728−8735.
(12) Kim, J. S.; Chang, W. S.; Kim, R. H.; Kim, D. Y.; Han, D. W.; Lee, K. H.; Lee, S. S.; Doo, S. G. High Capacity Nanostructured Manganese Dioxide Cathode for Rechargeable Magnesium Ion Batteries. *J. Power Sources* **2015**, *273*, 210−215.
(13) Tao, S.; Huang, W.; Liu, Y.; Chen, S.; Qian, B.; Song, L. Three Dimensional Hollow Spheres of the Tetragonal Spinel MgMn2O4 Cathode for High Performance Magnesium Ion Batteries. *J. Mater. Chem. A* **2018**, *6*, 8210−8214.
(14) Kim, C.; Phillips, P. J.; Key, B.; Yi, T.; Nordlund, D.; Yu, Y. S.; Bayliss, R. D.; Han, S. D.; He, M.; Zhang, Z.; Burrell, A. K.; Klie, R. F.; Cabana, J. Direct Observation of Reversible Magnesium Ion Intercalation into a Spinel Oxide Host. *Adv. Mater.* **2015**, *27*, 3377−3384.
(15) Tekin, B.; Demir cakan, R. Understanding the Role of Water Based Electrolytes on Magnesium Ion Insertion/Extraction into λ MnO2 Lattice Structure. *Solid State Ionics* **2019**, *335*, 67−73.
(16) Chen, W.; Zhan, X.; Luo, B.; Ou, Z.; Shih, P. C.; Yao, L.; Pidaparthy, S.; Patra, A.; An, H.; Braun, P. V.; Stephens, R. M.; Yang, H.; Zuo, J. M.; Chen, Q. Effects of Particle Size on Mg 2+ Ion Intercalation into λ MnO 2 Cathode Materials. *Nano Lett.* **2019**, *19*, 4712−4720.
(17) Hatakeyama, T.; Okamoto, N. L.; Shimokawa, K.; Li, H.; Nakao, A.; Uchimoto, Y.; Tanimura, H.; Kawaguchi, T.; Ichitsubo, T. Electrochemical Phase Transformation Accompanied with Mg Extraction and Insertion in a Spinel MgMn2O4 Cathode Material. *Phys. Chem. Chem. Phys.* **2019**, *21*, 23749−23757.
(18) Nam, K. W.; Kim, S.; Lee, S.; Salama, M.; Shterenberg, I.; Gofer, Y.; Kim, J. S.; Yang, E.; Park, C. S.; Kim, J. S.; Lee, S. S.; Chang, W. S.; Doo, S. G.; Jo, Y. N.; Jung, Y.; Aurbach, D.; Choi, J. W. The High Performance of Crystal Water Containing Manganese Birnessite Cathodes for Magnesium Batteries. *Nano Lett.* **2015**, *15*, 4071−4079.
(19) Sun, X.; Duffort, V.; Mehdi, B. L.; Browning, N. D.; Nazar, L. F. Investigation of the Mechanism of Mg Insertion in Birnessite in Nonaqueous and Aqueous Rechargeable Mg Ion Batteries. *Chem. Mater.* **2016**, *28*, 534−542.
(20) Kim, S.; Lee, S.; Nam, K. W.; Shin, J.; Lim, S. Y.; Cho, W.; Suzuki, K.; Oshima, Y.; Hirayama, M.; Kanno, R.; Choi, J. W. On the Mechanism of Crystal Water Insertion during Anomalous Spinel to Birnessite Phase Transition. *Chem. Mater.* **2016**, *28*, 5488−5494.
(21) Kim, S.; Nam, K. W.; Lee, S.; Cho, W.; Kim, J. S.; Kim, B. G.; Oshima, Y.; Kim, J. S.; Doo, S. G.; Chang, H.; Aurbach, D.; Choi, J. W. Direct Observation of an Anomalous Spinel to Layered Phase Transition Mediated by Crystal Water Intercalation. *Angew. Chem., Int. Ed.* **2015**, *54*, 15094−15099.
(22) Rasul, S.; Suzuki, S.; Yamaguchi, S.; Miyayama, M. High Capacity Positive Electrodes for Secondary Mg Ion Batteries. *Electrochim. Acta* **2012**, *82*, 243−249.
(23) Zhang, R.; Yu, X.; Nam, K. W.; Ling, C.; Arthur, T. S.; Song, W.; Knapp, A. M.; Ehrlich, S. N.; Yang, X. Q.; Matsui, M. α MnO2 as a Cathode Material for Rechargeable Mg Batteries. *Electrochem. Commun.* **2012**, *23*, 110−113.
(24) Zhang, R.; Arthur, T. S.; Ling, C.; Mizuno, F. Manganese Dioxides as Rechargeable Magnesium Battery Cathode; Synthetic Approach to Understand Magnesiation Process. *J. Power Sources* **2015**, *282*, 630−638.
(25) Arthur, T. S.; Zhang, R.; Ling, C.; Glans, P. A.; Fan, X.; Guo, J.; Mizuno, F. Understanding the Electrochemical Mechanism of K

AMnO2 for Magnesium Battery Cathodes. *ACS Appl. Mater. Interfaces* **2014**, *6*, 7004−7008.
(26) Ling, C.; Zhang, R.; Arthur, T. S.; Mizuno, F. How General Is the Conversion Reaction in Mg Battery Cathode: A Case Study of the Magnesiation of α MnO2. *Chem. Mater.* **2015**, *27*, 5799−5807.
(27) Kitchaev, D. A.; Dacek, S. T.; Sun, W.; Ceder, G. Thermodynamics of Phase Selection in MnO2 Framework Structures through Alkali Intercalation and Hydration. *J. Am. Chem. Soc.* **2017**, *139*, 2672−2681.
(28) Canepa, P.; Sai Gautam, G.; Hannah, D. C.; Malik, R.; Liu, M.; Gallagher, K. G.; Persson, K. A.; Ceder, G. Odyssey of Multivalent Cathode Materials: Open Questions and Future Challenges. *Chem. Rev.* **2017**, *117*, 4287−4341.
(29) Chabre, Y.; Pannetier, J. Structural and Electrochemical Properties of the Proton/γ MnO2 System. *Prog. Solid State Chem.* **1995**, *23*, 1−130.
(30) Ohzuku, T.; Kitagawa, M.; Hirai, T. Electrochemistry of Manganese Dioxide in Lithium Nonaqueous Cell: III. X Ray Diffractional Study on the Reduction of Spinel Related Manganese Dioxide. *J. Electrochem. Soc.* **1990**, *137*, 769−775.
(31) Shimokawa, K.; Atsumi, T.; Harada, M.; Ward, R. E.; Nakayama, M.; Kumagai, Y.; Oba, F.; Okamoto, N. L.; Kanamura, K.; Ichitsubo, T. Zinc Based Spinel Cathode Materials for Magnesium Rechargeable Batteries: Toward the Reversible Spinel Rocksalt Transition. *J. Mater. Chem. A* **2019**, *7*, 12225−12235.
(32) Li, H.; Okamoto, N. L.; Hatakeyama, T.; Kumagai, Y.; Oba, F.; Ichitsubo, T. Fast Diffusion of Multivalent Ions Facilitated by Concerted Interactions in Dual Ion Battery Systems. *Adv. Energy Mater.* **2018**, *8*, 1801475.
(33) Okamoto, N. L.; Shimokawa, K.; Tanimura, H.; Ichitsubo, T. Feasible Transformation of MgCo2O4 from Spinel to Defect Rocksalt Structure under Electron Irradiation. *Scr. Mater.* **2019**, *167*, 26−30.
(34) Thackeray, M. M.; Rossouw, M. H.; Gummow, R. J.; Liles, D. C.; Pearce, K.; de Kock, A.; David, W. I. F.; Hull, S. Ramsdellite MnO2 for Lithium Batteries: The Ramsdellite to Spinel Trans formation. *Electrochim. Acta* **1993**, *38*, 1259−1267.
(35) Verrelli, R.; Black, A. P.; Pattanathummasid, C.; Tchitchekova, D. S.; Ponrouch, A.; Oró Solé, J.; Frontera, C.; Bardé, F.; Rozier, P.; Palacín, M. R. On the Strange Case of Divalent Ions Intercalation in V2O5. *J. Power Sources* **2018**, *407*, 162−172.
(36) Kitchaev, D. A.; Peng, H.; Liu, Y.; Sun, J.; Perdew, J. P.; Ceder, G. Energetics of MnO2 Polymorphs in Density Functional Theory. *Phys. Rev. B: Condens. Matter Mater. Phys.* **2016**, *93*, 1−5.
(37) Ichitsubo, T.; Tokuda, K.; Yagi, S.; Kawamori, M.; Kawaguchi, T.; Doi, T.; Oishi, M.; Matsubara, E. Elastically Constrained Phase Separation Dynamics Competing with the Charge Process in the LiFePO4/FePO4 System. *J. Mater. Chem. A* **2013**, *1*, 2567−2577.
(38) Ichitsubo, T.; Doi, T.; Tokuda, K.; Matsubara, E.; Kida, T.; Kawaguchi, T.; Yagi, S.; Okada, S.; Yamaki, J. I. What Determines the Critical Size for Phase Separation in LiFePO4 in Lithium Ion Batteries? *J. Mater. Chem. A* **2013**, *1*, 14532−14537.
(39) Ichitsubo, T.; Yagi, S.; Doi, T.; Yukitani, S.; Hirai, K.; Matsubara, E. Influence of Mechanical Strain on the Electrochemical Lithiation of Aluminum Based Electrode Materials. *J. Electrochem. Soc.* **2011**, *159*, A14−A17.
(40) Baskin, A.; Prendergast, D. Ion Solvation Spectra": Free Energy Analysis of Solvation Structures of Multivalent Cations in Aprotic Solvents. *J. Phys. Chem. Lett.* **2019**, *10*, 4920−4928.
(41) Wan, L. F.; Prendergast, D. Ion Pair Dissociation on α MoO3 Surfaces: Focus on the Electrolyte Cathode Compatibility Issue in Mg Batteries. *J. Phys. Chem. C* **2018**, *122*, 398−405.
(42) Wang, X.; Li, Y. Selected Control Hydrothermal Synthesis of α and β MnO2 Single Crystal Nanowires. *J. Am. Chem. Soc.* **2002**, *124*, 2880−2881.
(43) Gaillot, A. C.; Flot, D.; Drits, V. A.; Manceau, A.; Burghammer, M.; Lanson, B. Structure of Synthetic K Rich Birnessite Obtained by High Temperature Decomposition of KMnO4. I. Two Layer Polytype from 800 °C Experiment. *Chem. Mater.* **2003**, *15*, 4666−4678.
(44) Kubota, K.; Nohira, T.; Goto, T.; Hagiwara, R. Ternary Phase Diagrams of Alkali Bis(Trifluoromethylsulfonyl)Amides. *J. Chem. Eng. Data* **2008**, *53*, 2144−2147.
(45) Kubota, K.; Nohira, T.; Hagiwara, R. Thermal Properties of Alkali Bis(Fluorosulfonyl)Amides and Their Binary Mixtures. *J. Chem. Eng. Data* **2010**, *55*, 3142−3146.
(46) Hagiwara, R.; Tamaki, K.; Kubota, K.; Goto, T.; Nohira, T. Thermal Properties of Mixed Alkali Bis(Trifluoromethylsulfonyl) Amides. *J. Chem. Eng. Data* **2008**, *53*, 355−358.
(47) Oishi, M.; Ichitsubo, T.; Okamoto, S.; Toyoda, S.; Matsubara, E.; Nohira, T.; Hagiwara, R. Electrochemical Behavior of Magnesium Alloys in Alkali Metal TFSA Ionic Liquid for Magnesium Battery Negative Electrode. *J. Electrochem. Soc.* **2014**, *161*, A943−A947.
(48) Momma, K.; Izumi, F. VESTA 3 for Three Dimensional Visualization of Crystal, Volumetric and Morphology Data. *J. Appl. Crystallogr.* **2011**, *44*, 1272−1276.
(49) Treacy, M. M. J.; Newsam, J. M.; Deem, M. W. A General Recursion Method for Calculating Diffracted Intensities from Crystals Containing Planar Faults. *Proceedings Royal Society of London, A* **1991**, *433*, 499−520.
(50) Blöchl, P. E. Projector Augmented Wave Method. *Phys. Rev. B: Condens. Matter Mater. Phys.* **1994**, *50*, 17953−17979.
(51) Kresse, G.; Furthmüller, J. Efficient Iterative Schemes for Ab Initio Total Energy Calculations Using a Plane Wave Basis Set. *Phys. Rev. B: Condens. Matter Mater. Phys.* **1996**, *54*, 11169−11186.
(52) Kresse, G.; Joubert, D. From Ultrasoft Pseudopotentials to the Projector Augmented Wave Method. *Phys. Rev. B: Condens. Matter Mater. Phys.* **1999**, *59*, 1758−1775.
(53) Perdew, J. P.; Burke, K.; Ernzerhof, M. Generalized Gradient Approximation Made Simple. *Phys. Rev. Lett.* **1996**, *77*, 3865−3868.
(54) Wang, L.; Maxisch, T.; Ceder, G. Oxidation Energies of Transition Metal Oxides within the GGA+U Framework. *Phys. Rev. B: Condens. Matter Mater. Phys.* **2006**, *73*, 1−6.
(55) van de Walle, A.; Ceder, G. Automating First Principles Phase Diagram Calculations. *J. Phase Equilib.* **2002**, *23*, 348−359.
(56) Van de Walle, A.; Asta, M.; Ceder, G. The Alloy Theoretic Automated Toolkit: A User Guide. *CALPHAD: Comput. Coupling Phase Diagrams Thermochem.* **2002**, *26*, 539−553.